Carbon 202 (2023) 207–213

Contents lists available at ScienceDirect

Carbon

journal homepage: www.elsevier.com/locate/carbon

Rare earth free oxide nano-composite of $SrTi_{0.85}Nb_{0.15}O_3$ and CNT for potential n-type thermoelectrics

Subhra Sourav Jana, Tanmoy Maiti *

Plasmonics and Perovskites Laboratory, Department of Materials Science and Engineering, IIT Kanpur, U.P, 208016, India

A B S T R A C T

Despite having large electron concentration, the electrical conductivity of Nb doped $SrTiO_3$ severely suffers from poor carrier mobility. Even after taking several attempts by different research groups, it is still challenging to improve carrier mobility without affecting the Seebeck coefficient. In this report, 1-dimensional CNT has been introduced in $SrTi_{0.85}Nb_{0.15}O_3$ (STN) matrix to fabricate STN + CNT nano composites as CNT is expected to have boosted the mobility by several orders. We have reported more than 1000 % increase in electrical conductivity after CNT addition. In contrast, Seebeck coefficient remains flat with CNT loading. This remarkable enhancement of electrical conductivity accompanied by essentially no change in thermopower leads to a 380 % increase in the *ZT* parameter. Although CNT has been previously introduced in chalcogenides, binary oxides, and oxy-chalcogenides, such a remarkable surge in electrical transport with the incorporation of a small amount of CNT has never been reported. Moreover, to the best of our knowledge, this is the first report on thermoelectric properties of oxide perovskite composites with CNT. Our results suggest that forming oxide-CNT nano-composites can be a robust strategy to improve the thermoelectric performance in bulk materials for realistic applications.

1. Introduction

Thermoelectric power generator has been in use for decades in spacecraft utilizing constant heat sources in radio-isotope thermoelectric generator (RTG) [1,2]. Further, a lot of efforts have been recently made in the development of thermoelectric generators, especially the computationally assisted technique to design the targeted thermoelectric generators such as in medical devices, flexible electronics, solid-state refrigeration etc. [3–5] In the last two decades, the concept of waste heat recovery by TEG has piqued the interest as a mean of combating the global energy crisis and environmental concerns. The dimensionless figure of merit, ZT ($= \frac{S^2\sigma}{\kappa} T$) determines the performance of thermoelectric materials, where S, σ and κ are Seebeck coefficient, electrical and thermal conductivity respectively. Ideally, high ZT is achieved in a thermoelectric material when it shows large σ, large S and low κ, which is difficult to coexist due to their interdependencies. Formerly, oxides have not been considered as good candidates for thermoelectric applications due to their poor electrical conductivity and large thermal conductivity compared to state-of-the-art chalcogenides. Nonetheless, oxide thermoelectrics have certain advantages over chalcogenides, such as high temperature stability, non-toxic constituents, and low processing cost [6]. $SrTiO_3$ (STO) has received extensive attention as a leading n-type oxide thermoelectric material due to its large Seebeck coefficient ($\sim 850\mu VK^{-1}$) and tunable electrical conductivity [7]. Pristine STO shows very poor electrical conductivity with electron concentration, $n < 10^{15}cm^{-3}$ [8]. Nb^{5+}doped STO (STN) has been proven to be one of the potential thermoelectric candidates because of its large carrier concentration with a reasonably high Seebeck coefficient [9–11]. However, this donor doped STO exhibits low electrical conductivity despite possessing a large electron concentration on the order of $\sim 10^{21}cm^{-3}$. It is believed that the presence of multivalent cations in ABO_3 perovskite oxides causes a variation in local electronic charge and lattice strain, giving rise to localization of electrons, called Anderson localization [12–19]. Because of which, the mobility of electrons gets suppressed in these complex oxides. In addition, this behavior is coupled with a high thermal conductivity, causing a deterioration of their thermoelectric performance. Recently, researchers have found that incorporation of graphite in donor doped STO can help these localized electrons to become delocalized, resulting in enhanced electron mobility [18,19]. This helps the STN + graphite composite attain a groundbreaking ZT value of 1.42 for n-type bulk oxide thermoelectric [18].

In the present work, multiwalled carbon nanotube (CNT) has been introduced in STN matrix as a mobility enhancer. CNT is expected to help in delocalizing the localized electrons in STN by generating high momentum electrons. CNT, especially multiwalled CNT, is known for its high aspect ratios with nano-size dimensionality and its multichannel quasi-ballistic electrical conductivity of $1.85 \times 10^5 Sm^{-1}$ [20,21]. Few reports have been found on CNT based composites with chalcogenides

* Corresponding author.
E-mail address: tmaiti@iitk.ac.in (T. Maiti).

https://doi.org/10.1016/j.carbon.2022.11.039
Received 13 August 2022; Received in revised form 3 October 2022; Accepted 15 November 2022
Available online 22 November 2022

such as Bi_2Te_3, SnSe, Cu_2Se, Ag_2Se showing a moderate improvement in thermoelectric figure of merit, with the reason being primarily demonstrated as suppressed lattice thermal conductivity due to the phonon scattering at the newly formed CNT-matrix interfaces [22–26]. Additionally, it has been found that electrical conductivity is slightly improved as CNT acts as the 'bridges' between the grains to accelerate electrons [22,24]. In contrast, a few other reports suggest that electrical conductivity is slightly suppressed due to carrier scattering at CNT-matrix interfaces [23,25,26]. However, no such work on STO-based CNT composites has been reported till date.

In the present work, nano-composites of $SrTi_{0.85}Nb_{0.15}O_3$ (STN)+ CNT have been fabricated using spark plasma sintering (SPS). Being an excellent conductor, CNT acts as an electron accelerator, increasing the electrical conductivity of the STN + CNT composites by 11 times than that of pristine STN without any negative impact on Seebeck coefficient. We have reported more than 4 times augmentation in *ZT* values for STN + CNT composites with respect to pristine STN. Such a robust thermoelectric performance for n-type thermoelectric oxides is quite promising for high temperature applications.

2. Experimental

2.1. Material synthesis and STN + CNT composite formation

$SrTi_{0.85}Nb_{0.15}O_3$ (STN) is synthesized by mixing stoichiometric ratio of raw materials, namely $SrCO_3$ (99.9% purity, Sigma Aldrich), TiO_2 (99.9% purity, Sigma Aldrich), Nb_2O_5 (99.9% purity, Sigma Aldrich). The mixture is calcined 4–5 times in reducing atmosphere at 1400°*C*–1500°*C* with intermediate grinding steps. Once the single phase (STN) is obtained, it is mixed with different wt% (0.3, 0.5, 1, 1.5) of Multi walled CNT powder (> 98% purity) followed by high energy ball milling at 600 rpm for better dispersion of CNT. Finally, STN + CNT powder is consolidated using spark plasma sintering (SPS) at 1400°*C* using 30 Mpa pressure. These pellets are cut and machined into required dimensions for all the characterizations.

2.2. Material characterization

Phase and microstructure have been analysed using X-Ray Diffraction (PAN ANALYTICAL, ACMS, IITK), FESEM, Electron Backscatter Diffraction (JSM-7100F, JEOL, IITK), TEM (FEI-Tecnai G2 12 Twin 120 KV TEM, AIC, IITK), X-ray Photoelectron Spectroscopy (PHI 5000 Versa Probe II, FEI Inc.), Raman Sepectroscopy (532*nm* DPSS laser, PRINCETON INSTRUMENT ACTON SERIES SP 2500I SPECTROSCOPE). Seebeck and Electrical conductivity have been measured using ZEM-3M10R, ULVAC-RICO Inc. apparatus. Thermal diffusivity and specific heat capacity have been estimated from TC-1200RH and ADVANCE RIKO and HDSC PT 1600 (LINSEIS), respectively. carrier concentration measurement has been performed in HMS-5000 Series Hall Effect measurement system, Ecopia, ACMS, IITK).

3. Results and discussions

3.1. Microstructure and phase analysis

STN + CNT composites have been synthesized by the solid-state

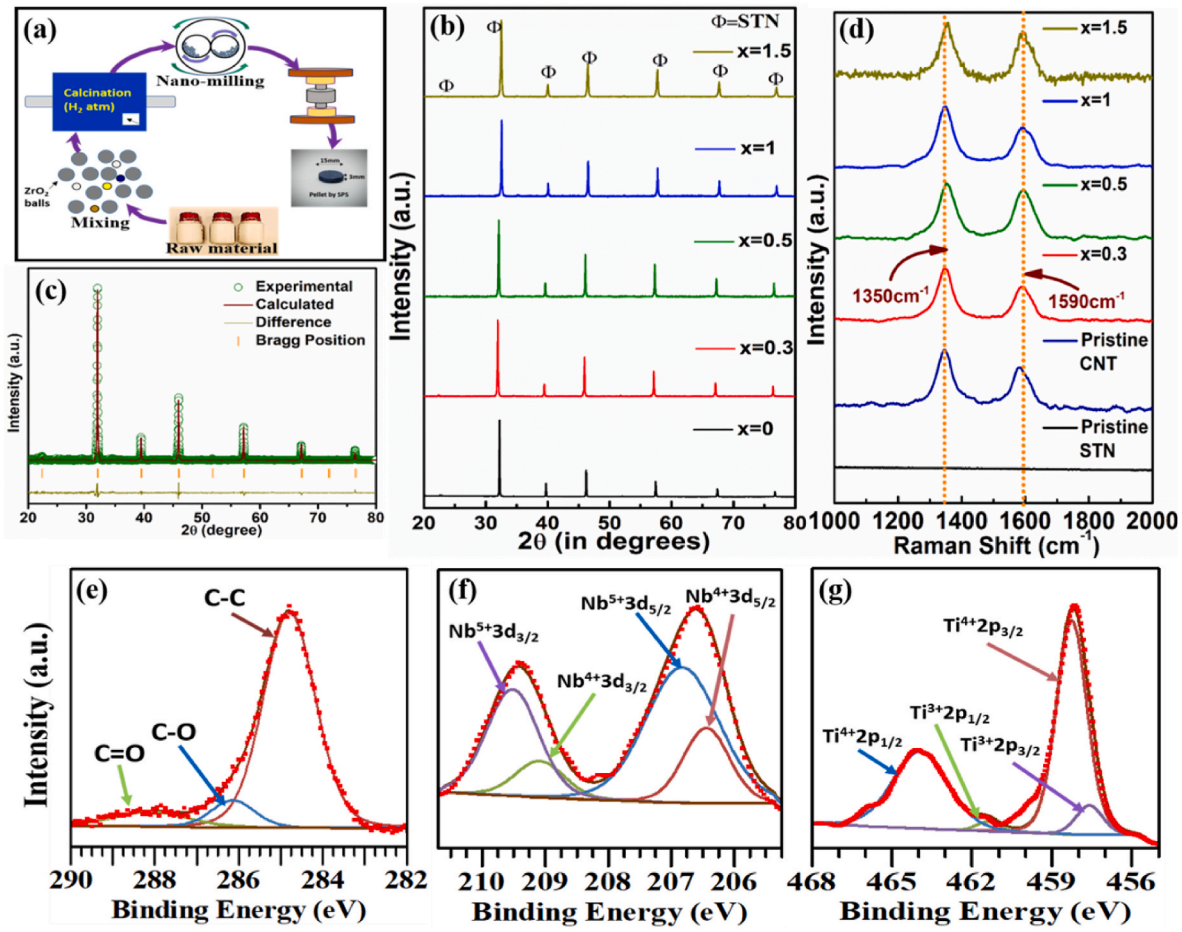

Fig. 1. (a) Schematics of the composite processing (b) XRD of STN + CNT composites (c) Rietveld refinement of STN+0.5 wt% CNT (d) Raman spectroscopy of STN + CNT (e–g) XPS spectra of STN+0.5 wt% CNT. (A colour version of this figure can be viewed online.)

route and consolidated using spark plasma sintering (SPS). Fig. 1(a) demonstrates the schematics of processing steps. An XRD analysis of all the compositions is shown in Fig. 1(b), where all the peaks are fully indexed with cubic $Pm\bar{3}m$ space group. STN with cubic perovskite structure has been retained throughout different CNT concentrations. Rietveld refinement has been performed to estimate the lattice parameters of all the composites, as shown in Fig. 1(c) and **table (S1& S2)**. The lattice parameter of 3.92 Å has been found for pristine STN and it doesn't change much after CNT addition. However, no XRD peak has been detected corresponding to the CNT phase due to its low concentration [27]. The presence of CNT has been identified by Raman spectroscopy as shown in Fig. 1(d). The peaks at 1350 cm^{-1} and 1590 cm^{-1} correspond to the high frequency D mode and low frequency G mode of CNT, respectively [28]. These D and G bands are related to the vibration frequency of sp^3 and sp^2 hybridized carbons [29,30]. It is to be noted that the intensity ratio between the D and G bands (I_D/I_G) of STN + CNT composites remains identical to pristine CNT, implying that CNT has not been considerably damaged throughout the severe processing steps. Moreover, there is no peak shift of D and G bands, indicating that CNT does not react or decompose during the processing.

X-ray photoelectron spectroscopy (XPS) has been performed to verify the oxidation states and binding energies of C, Nb, Ti and O. Fig. 1(e-g) provides the detailed peak fittings and corresponding binding energies are tabulated in SI (Table S3)). The binding energies are in good agreement with the literature values [31–35]. The deconvolution of carbon spectra confirms that the most of the carbon (~ 83 %) in CNT remains in graphitic bond (C–C bond). Some of the carbon has been found in the form of C–O bond C═O bond as expected due to the extreme processing steps such as nano-milling. XPS spectra of Nb reveals that around 76% of the Nb remains in the +5 state, which acts as donor dopant, whereas more than 90% of the Ti remains in the +4 state.

Furthermore, the FESEM image of the fractured surface in Fig. 2(a) demonstrates that STN + CNT composites possess a sufficiently dense micro-structure. As indicated by yellow arrow in Fig. 2(a), CNTs are mostly found uniformly distributed at grain boundaries. Presence of CNT in the grain boundaries is further confirmed using energy dispersive x-ray spectroscopy (EDXS) as shown in Fig. 2(b). Elemental mapping by EDXS also confirms that all the constituent elements are homogeneously distributed throughout the microstructure, as shown in Fig. S1(a-e). The grain size distribution of STN + CNT composites has been estimated from bright field image of electron back scattered diffraction (EBSD), as shown in (Fig. 2(c) & Fig. S2). It has been found that about 70% of the total grains in STN+0.5 wt% CNT are in the size below 100 *nm* and less than 2% are above 700 *μm*. This wide range of grain size distribution is an ideal recipe to facilitate charge transport through large grains and enhance phonon scattering by grain boundaries. However, CNT is very prone to forming agglomerates because of its high surface energy. The pockets of CNT bundles become more prominent as the CNT concentration increases, as shown in the phase contrast image in Fig. 2(d). To find out more about distribution of CNT in STN matrix TEM imaging has been performed. The d-spacing of two yellow circled regions in Fig. 2(e) has been calculated as 2.73Å and 3.36Å using the fast Fourier transform (FFT), and can be indexed with the planes of STN [110] and CNT [$11\bar{2}0$], respectively. Fig. 2(e) also shows two distinct areas separated by yellow dotted line labelled STN grains surrounded by CNT. The existence of CNT in the STN matrix is further illustrated schematically in Fig. 2(f)

3.2. Electrical transport

Temperature dependent Seebeck coefficient and electrical conductivity have been measured in the broad temperature range from 330 *K* to 990 *K* to evaluate the electrical transport in STN + CNT composites, as shown in Fig. 3((a) & (b)). The negative Seebeck coefficient for all the compositions across the temperature range indicates that the electron is the major carrier in the composites. Linear increase of the Seebeck coefficient ranging approximately from 75 μV to 181 μV with temperature for all the compositions depicts n-type degenerate semiconductor behavior. The inclusion of CNTs has been shown to have minimal effects on the Seebeck coefficient of STN, as illustrated in the inset of Fig. 3(a). It is quite advantageous to obtain nearly identical Seebeck values even with CNT inclusions in STN, especially given that the CNT actually increases the electrical conductivity of STN by an order of magnitude, as will be covered below.

Electrical conductivity is enhanced to 1.7×10^5 Sm^{-1} for 0.5 wt % CNT, which is more than 1000% larger compared to that of pristine STN. Although CNT possesses large electrical conductivity in the order of 10^5 Sm^{-1} [20,36,37] due to its large quasi-ballistic electrical transport, such a huge surge in electrical conductivity of STN due to less than 1 *vol*% CNT incorporation is difficult to perceive. This order of magnitude surge in electrical conductivity without sacrificing the Seebeck coefficient helps to achieve a maximum power factor of

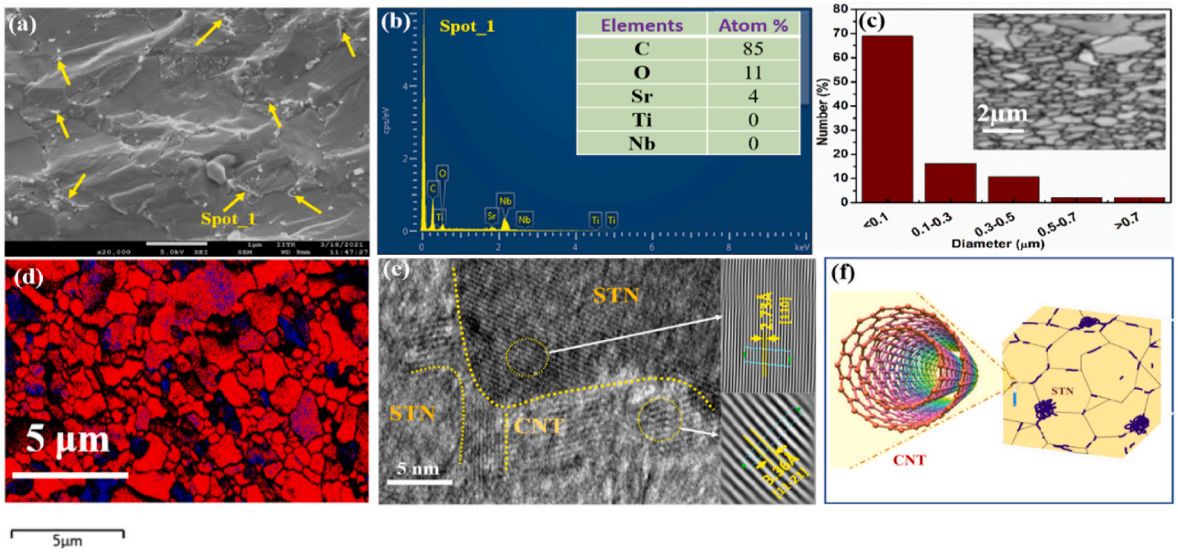

Fig. 2. Microstructural study (a) FESEM of fractured surface (b) EDXS data (c) grain size distribution with bright field image at the inset (d) Phase contrast image, red and blue regions depicting STN and CNT, respectively (e) TEM analysis of STN+0.5 wt% CNT (f) Schematics of the CNT distribution in the matrix of STN. (A colour version of this figure can be viewed online.)

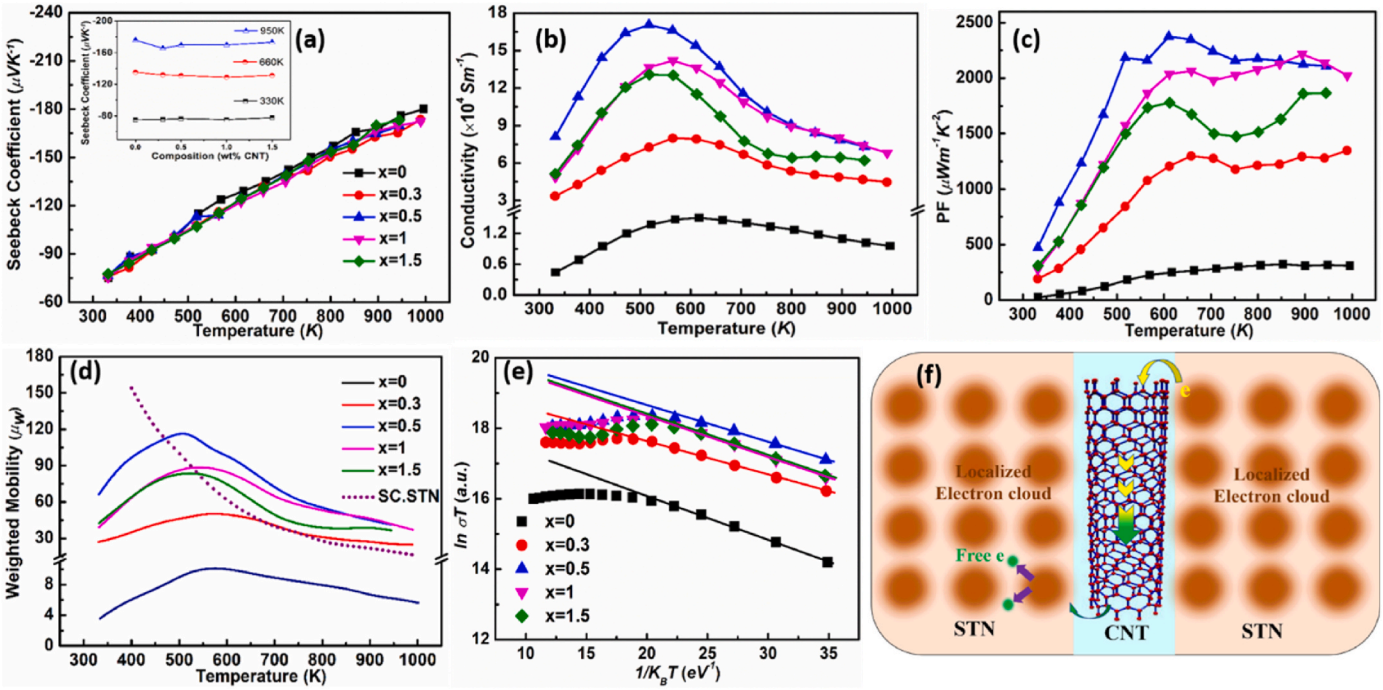

Fig. 3. Electrical transport (a) Seebeck coefficient with temperature (with composition in inset) (b) electrical conductivity (c) power factor (d) weighted mobility (μ_w) of STN + CNT composites in comparison to single crystal (SC-STN) [38] (e) $\ln(\sigma T)$ vs. $^{1}/_{K_B T}$ (f) Schematics of the electron transport depicting momentum enhancement by transfer of electron through CNT in the sintered STN + CNT composites.

2375 $\mu W m^{-1} K^{-2}$ for STN+0.5 wt% CNT composition, which is around 635 % larger than that of pristine STN. Being a degenerate type semiconductor, fermi energy is most likely to be located within the conduction band edge, and therefore, it should follow metallic-like behavior. But it is surprising to observe semiconductor like behavior at lower temperature regions before it undergoes a semiconductor ($d\sigma/dT > 0$) to metal-like ($d\sigma/dT < 0$) transition at 500 $K-$ 600 K as listed in Table S5.

To investigate the insight of electronic transport, carrier concentration has been estimated using four probe Hall measurements at room temperature. The electron concentration for all the compositions as shown in Table S4 is found to be in the range $(4-5) \times 10^{20} cm^{-3}$ indicating not much variation in carrier concentration, which cannot justify such a huge enhancement in electrical conductivity. Furthermore, using the Pisarenko relation, DOS effective mass is found to be in the range of 1.8 to 2.2 in Fig. S3 and it doesn't vary much as well with CNT addition. Minimal deviation in DOS effective mass and electron concentration corroborates well with the identical Seebeck coefficient for different compositions, but the order of magnitude surge in σ still remains unanswered.

To better comprehend the optimization of electronic properties, carrier concentration independent weighted mobility (μ_w) [39–42] as shown in Fig. 3(d) has been computed for all the compositions using Seebeck and electrical conductivity using equation (S2) in SI. Electron mobility of STN has been found to be increased dramatically due to the incorporation of CNT in the STN matrix. Most importantly, the same order of increment in μ_w has been obtained as what we have obtained in σ. Maximum μ_w of 120 $cm^2 V^{-1} S^{-1}$ has been achieved for STN+0.5 wt% CNT which is 1000% larger in comparison to that of pristine STN. It infers that such an enhanced μ_w is the main attributor to the aforementioned increase in electrical conductivity.

Positive slop of μ_w at lower temperatures suggests thermally activated mobility. Some previous literatures attribute the large enhancement in σ in STN + r-GO composites to the reduction in Schottky barrier height as r-GO promotes formation of more oxygen vacancies in the vicinity of the grain boundaries [43–45]. Although this hypothesis is not fully refutable for well-dispersed CNT composites, it is difficult to perceive this mechanism as the primary cause of the spectacular enhancement in weighted mobility, even higher than that of the single crystal [44,46]. Moreover, it fails to justify almost no change in the Seebeck coefficient for all the compositions as oxygen vacancies supply more electrons to the conduction band owing to its behavior as an electron donor dopant [47–51]. The band model cannot adequately explain the charge transport mechanism in these complex oxide perovskites, which contain point defects due to the presence of multivalent cations and high temperature (>1400 K) ceramic processing. Furthermore, the percolation model doesn't appear to operate in this instance, as the passage of a large number of electrons through CNT is expected to have deteriorated the Seebeck coefficient [52]. In addition, it is very unusual that the STN + CNT composites, including the pristine STN, exhibit semiconductor like behavior at lower temperature regions despite possessing larger carrier concentration than the critical concentration required to satisfy the Mott criteria for $SrTiO_3$ based oxides ($10^{18} cm^{-3}$) [53]. Based on our prior research, it is posited here that localization of electrons called Anderson localization, which has been observed in many complex oxides, could be a possible reason behind the poor electronic conductivity of the pristine STN despite its large electron concentration [54–56]. Nb doping in the B site, repeated calcination in a reducing atmosphere, and nano-milling can all generate a lot of defects and lattice strain, giving rise to a difference in local electric field causing localization of electrons. As a result, small polaron hopping (SPH) can be found as a dominant electron transport mechanism at lower temperature regions, as shown in Fig. 3(e). This explains the thermally activated charge transport leading to semiconductor like electrical conductivity ($d\sigma/dT > 0$) in STN + CNT composites. The activation energy (E_{hop}) for SPH (Table S6) has been found to be decreasing with a little addition of CNT, as determined from linear fitting of $ln(\sigma)$ with $^{1}/_{K_B T}$ in equation (1).

$$\sigma = \frac{\sigma_0}{T} exp\left(-\frac{E_{Hop}}{K_B T}\right) \quad (1)$$

Where, σ_0 and T_0 are constants. Further, one-dimensional CNT serves as an electron mobility booster by providing a conductive channel for ballistic electron transport [57]. The intrinsic electron mobility of CNT at room temperature is in the range of $> 10^3\ cm^2V^{-1}S^{-1}$ [58–60]. As a result, electrons coming out of CNT are expected to achieve high momentum. In addition to the supply of high energy electrons from CNT to STN, the presence of CNT in the composites is expected to impart enough strain to help the localized electrons in STN to attain an itinerant state, as shown schematically in Fig. 3(f). Meanwhile, the overall electron concentration is not influenced; hence, it remains undetectable by the Hall measurement technique. Although CNT possesses a large electron concentration as estimated to be around $10^{20} - 10^{22}\ cm^{-3}$ [58–60], it is unable to influence the overall electron concentration of STN + CNT composites as STN already contains surplus of electrons (on the order of $10^{21}\ cm^{-3}$). Moreover, such a low content of CNT (1– 2 %) is not in fact expected to affect the overall electron concentration of STN + CNT composites. As a result, overall Seebeck coefficient remains almost unaltered even after CNT addition because of its independence on the state of electrons, i.e., whether they are localized or itinerant [61]. Formation of CNT agglomerates cannot be ignored as it has a large tendency to form bundles as observed in Fig. 2(d). Eventually, electron scattering begins to dominate at larger CNT concentrations (>0.5 wt%), reflected through a slightly larger value of m^* for STN+2 wt% CNT. This is also consistent with the μ_w reduction at large CNT concentrations because of which electrical conductivity is suppressed.

3.3. Thermal transport

The total thermal conductivity in Fig. 4(a) has been determined by measuring thermal diffusivity, specific heat, and density, as depicted in Fig. S4 and Table S7 in SI. Even though CNTs possess a very large thermal conductivity of about 2000 $Wm^{-1}K^{-1}$, the κ_{total} of all the STN + CNT composites exhibits a minimal increase with respect to pristine STN [37,62]. To evaluate the thermal transport phenomena in detail, κ_e has been estimated using the Wiedemann-Franz law ($\kappa_e = L\sigma T$) as shown in SI [63]. The temperature dependent κ_e has been found to be a replica of electrical conductivity, as shown in Fig. S4(d). Further, lattice thermal conductivity (κ_l) has been calculated by subtracting κ_e from the total thermal conductivity as shown in Fig. 4(b). Temperature dependent κ_l of all the STN + CNT composites remain range bound between 6.5 $Wm^{-1}K^{-1}$ to 2.8 $Wm^{-1}K^{-1}$. The monotonically decreasing trend of κ_l with temperature for all the compositions suggests the dominance of phonon-phonon Umklapp scattering at high temperature regions. This phenomenon has already been reported in several oxide composites [18,19,64–66]. It is worth noting that despite ~10 times increase in κ_e as expected due to an order of magnitude increase in electrical conductivity, κ_{total} could be restricted since the overall thermal conductivity is dominated by lattice thermal conductivity (κ_l); hence, the curvature of κ_e is overshadowed by κ_l. However, unlike graphene and graphite, CNT doesn't work effectively to suppress the κ_l significantly suggesting that phonon doesn't scatter much in the interfaces of 1-dimensional CNT with STN grains. However, κ_l is not enhanced too much if it is considered with a 635% increase in PF after CNT loading.

3.4. Thermoelectric performance

Finally, the dimensionless figure of merit, *ZT*, has been computed in Fig. 4(c), where the maximum *ZT* of 0.48 has been found for STN+0.5 wt % CNT at 945 *K* which is also attained by STN+1 wt% CNT near 990 *K* temperature. The highest *ZT* value of the STN + CNT composite is about 340% larger than that of pristine STN. The maximum theoretical efficiency (η_{max}) is further calculated using equation (2&3) [67].

$$\eta_{max} = \eta_c \frac{\sqrt{1 + Z\,T_{avg}} - 1}{\sqrt{1 + Z\,T_{avg}} + \frac{T_c}{T_h}} \tag{2}$$

$$ZT_{avg} = \frac{\int_{T_c}^{T_h} ZT(T)dT}{T_h - T_c} \tag{3}$$

Where, η_c, T_c, T_h are Carnot efficiency, cold and hot end temperatures, respectively. From equation (2&3), it is evident that ZT_{avg} is more important parameter than maximum *ZT* in terms of its practical implication in actual TEG devices. ZT_{avg} of all the STN + CNT composites are

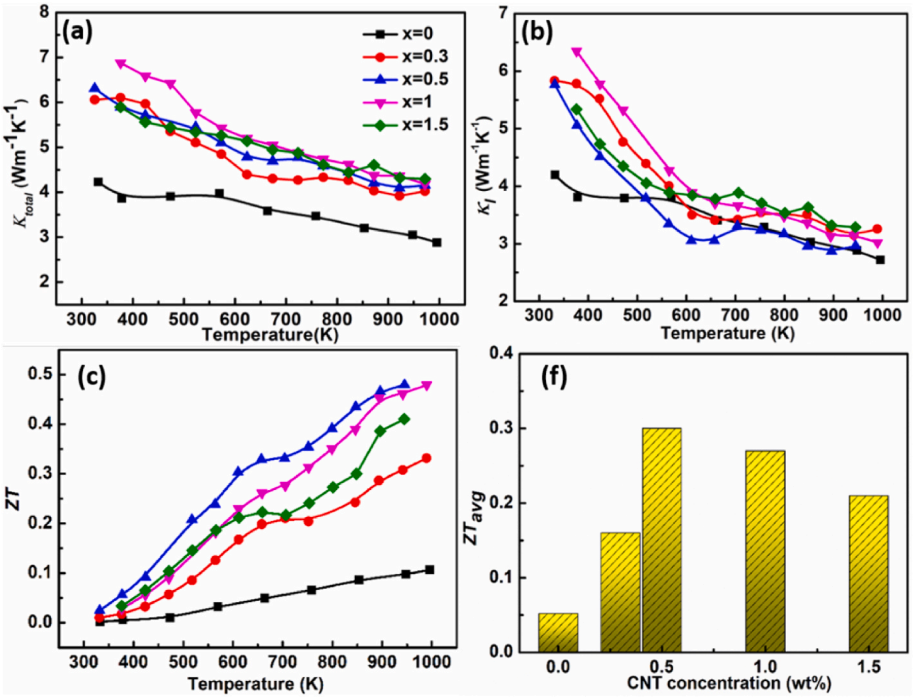

Fig. 4. Thermal transport and figure of merit (a) κ_{total} with temperature (b) κ_l with temperature (c) *ZT* with temperature (d) ZT_{avg} with temperature for all STN + CNT composites.

estimated in Fig. 4(d). Maximum ZT_{avg} of 0.3 has been obtained by STN+0.5 wt% CNT in the temperature range of 330 K − 990 K, yielding a maximum theoretically attainable efficiency of 6.6%, making it a potential option to be utilized in high temperature TEG applications. This can create a new opportunity for the development of TEG device using high performance oxide-CNT composites. Moreover, other high-performance oxides can be further utilized to form CNT based composites in the quest for next generation potential thermoelectric material.

4. Conclusion

In summary, we have successfully synthesized STN + CNT nanocomposites using spark plasma sintering. As confirmed by FESEM and TEM, CNTs are distributed in grain boundary regions. The presence of CNT in STN matrix offers high energy electrons, resulting in a remarkable enhancement in the electron mobility, which would otherwise suffer from Anderson localization of electrons. We have reported a maximum 1000 % surge in weighted mobility without any significant deterioration in thermopower for STN + CNT composite compared to that of pristine STN. As a result, a maximum ZT of 0.48 has been obtained for STN+0.5 wt% CNT at 945 K, which is around 380% larger than that of the pristine STN. In this work, we have shown a strategy of oxide-CNT nanocomposite formation for enhanced thermoelectric performance, where 1-D CNT acts as a mobility enhancer.

CRediT authorship contribution statement

Subhra Sourav Jana: Formal analysis, Writing – original draft, synthesized the samples and performed all the experiments. analysed the data and wrote the main manuscript with the help of. **Tanmoy Maiti:** was responsible for the original research concept and physical interpretation.

Declaration of competing interest

The authors declare that they have no known competing financial interests or personal relationships that could have appeared to influence the work reported in this paper.

Acknowledgement

This work is supported by the grant from Science and Engineering Research Board, DST (SERB-DST), India (Grant No: IMP/20l8/000955).

Appendix A. Supplementary data

Supplementary data to this article can be found online at https://doi.org/10.1016/j.carbon.2022.11.039.

References

[1] L.E. Bell, Cooling, heating, generating power, and recovering waste heat with thermoelectric systems, Science 321 (5895) (2008) 1457–1461.
[2] G.J. Snyder, E.R. Toberer, rafNP Group, Complex thermoelectric materials, Nat. Mater. 7 (2) (2011) 101–110.
[3] W.Y. Chen, X.L. Shi, J. Zou, Z.G. Chen, Thermoelectric coolers for on-chip thermal management: materials, design, and optimization, Mater. Sci. Eng. R Rep. 151 (2022), 100700.
[4] T. Cao, X.L. Shi, Z.G. Chen, Advances in the design and assembly of flexible thermoelectric device, Prog. Mater. Sci. (2022), 101003.
[5] B. Hu, X.L. Shi, J. Zou, Z.G. Chen, Thermoelectrics for medical applications: progress, challenges, and perspectives, Chem. Eng. J. (2022), 135268.
[6] G. Tan, L.D. Zhao, M.G. Kanatzidis, Rationally designing high-performance bulk thermoelectric materials, Chem. Rev. 116 (19) (2016) 12123–12149.
[7] H. Ohta, K. Sugiura, K. Koumoto, Recent progress in oxide thermoelectric materials: p-type Ca3Co4O9 and n-type SrTiO3, Inorg. Chem. 47 (19) (2008) 8429–8436.
[8] H. Ohta, Thermoelectrics based on strontium titanate, Mater. Today 10 (10) (2007) 44–49.
[9] A. Tkach, J. Resende, K.V. Saravanan, M.E. Costa, P. Diaz-Chao, E. Guilmeau, O. Okhay, P.M. Vilarinho, Abnormal grain growth as a method to enhance the thermoelectric performance of Nb-doped strontium titanate ceramics, ACS Sustain. Chem. Eng. 6 (12) (2018) 15988–15994.
[10] J. Wang, B.Y. Zhang, H.J. Kang, Y. Li, X. Yaer, J.F. Li, Q. Tan, S. Zhang, G.H. Fan, C. Y. Liu, L. Miao, Record high thermoelectric performance in bulk SrTiO3 via nano-scale modulation doping, Nano Energy 35 (2017) 387–395.
[11] B. Zhang, J. Wang, T. Zou, S. Zhang, X. Yaer, N. Ding, C. Liu, L. Miao, Y. Li, Y. Wu, High thermoelectric performance of Nb-doped SrTiO 3 bulk materials with different doping levels, J. Mater. Chem. C 3 (43) (2015) 11406–11411.
[12] A. Biswas, K.S. Kim, Y.H. Jeong, Metal insulator transitions in perovskite SrIrO3 thin films, J. Appl. Phys. 116 (21) (2014), 213704.
[13] S.R. Gilbert, L.A. Wills, B.W. Wessels, J.L. Schindler, J.A. Thomas, C.R. Kannewurf, Electrical transport properties of epitaxial BaTiO3 thin films, J. Appl. Phys. 80 (2) (1996) 969–977.
[14] Y. Li, J. Liu, J.C. Li, Y.F. Chen, X.M. Zhang, X.J. Wang, F.N. Wang, W.B. Su, L. L. Zhao, C.L. Wang, Electron localization in niobium doped CaMnO 3 due to the energy difference of electronic states of Mn and Nb, Phys. Chem. Chem. Phys. 20 (31) (2018) 20571–20574.
[15] S. Lee, J.A. Bock, S. Trolier-McKinstry, C.A. Randall, Ferroelectric-thermoelectricity and Mott transition of ferroelectric oxides with high electronic conductivity, J. Eur. Ceram. Soc. 32 (16) (2012) 3971–3988.
[16] T. Maiti, M. Saxena, P. Roy, Double perovskite (Sr 2 B′ B ″O 6) oxides for high-temperature thermoelectric power generation—a review, J. Mater. Res. (2018) 1–19.
[17] P. Roy, V. Waghmare, K. Tanwar, T. Maiti, Large change in thermopower with temperature driven p–n type conduction switching in environment friendly Ba x Sr 2− x Ti 0.8 Fe 0.8 Nb 0.4 O 6 double perovskites, Phys. Chem. Chem. Phys. 19 (8) (2017) 5818–5829.
[18] M. Acharya, S.S. Jana, M. Ranjan, T. Maiti, High performance (ZT> 1) n-type oxide thermoelectric composites from earth abundant materials, Nano Energy 84 (2021), 105905.
[19] S.S. Jana, T. Maiti, Interfaces, enhanced thermoelectric performance in oxide composites of La and Nb codoped SrTiO3 by using graphite as the electron mobility booster, ACS Appl. Mater. Interfaces (2022) 14174–14181.
[20] H. Li, W.G. Lu, J.J. Li, X.D. Bai, C.Z. Gu, Multichannel ballistic transport in multiwall carbon nanotubes, Phys. Rev. Lett. 95 (8) (2005), 086601.
[21] K. Ahmad, W. Pan, Dramatic effect of multiwalled carbon nanotubes on the electrical properties of alumina based ceramic nanocomposites, Compos. Sci. Technol. 69 (7–8) (2009) 1016–1021.
[22] X.Y. Mao, X.L. Shi, L.C. Zhai, W.D. Liu, Y.X. Chen, H. Gao, M. Li, D.Z. Wang, H. Wu, Z.H. Zheng, Y.F. Wang, High thermoelectric and mechanical performance in the n-type polycrystalline SnSe incorporated with multi-walled carbon nanotubes, J. Mater. Sci. Technol. 114 (2022) 55–61.
[23] K.T. Kim, S.Y. Choi, E.H. Shin, K.S. Moon, H.Y. Koo, G.G. Lee, G.H. Ha, The influence of CNTs on the thermoelectric properties of a CNT/Bi2Te3 composite, Carbon 52 (2013) 541–549.
[24] L. Zhao, S.M. Islam, J. Wang, D.L. Cortie, X. Wang, Z. Cheng, J. Wang, N. Ye, S. Dou, X. Shi, L. Chen, Significant enhancement of figure-of-merit in carbon-reinforced Cu2Se nanocrystalline solids, Nano Energy 41 (2017) 164–171.
[25] R. Nunna, P. Qiu, M. Yin, H. Chen, R. Hanus, Q. Song, T. Zhang, M.Y. Chou, M. T. Agne, J. He, G.J. Snyder, Ultrahigh thermoelectric performance in Cu 2 Se-based hybrid materials with highly dispersed molecular CNTs, Energy Environ. Sci. 10 (9) (2017) 1928–1935.
[26] H. Wang, X. Liu, Z. Zhou, H. Wu, Y. Chen, B. Zhang, G. Wang, X. Zhou, G. Han, Constructing n-type Ag2Se/CNTs composites toward synergistically enhanced thermoelectric and mechanical performance, Acta Mater. 223 (2022), 117502.
[27] A.Q. Xie, J. Guo, L. Zhu, S. Chen, Carbon dots promoted photonic crystal for optical information storage and sensing, Chem. Eng. J. 415 (2021), 128950.
[28] V.L. Kuznetsov, S.N. Bokova-Sirosh, S.I. Moseenkov, A.V. Ishchenko, D. V. Krasnikov, M.A. Kazakova, A.I. Romanenko, E.N. Tkachev, E.D. Obraztsova, Raman spectra for characterization of defective CVD multi-walled carbon nanotubes, Phys. Status Solidi 251 (12) (2014) 2444–2450.
[29] G. Wang, J. Yang, J. Park, X. Gou, B. Wang, H. Liu, J. Yao, Facile synthesis and characterization of graphene nanosheets, J. Phys. Chem. C 112 (22) (2008) 8192–8195.
[30] C. Rao, A.E. Sood, K.E. Subrahmanyam, A. Govindaraj, Graphene: the new two-dimensional nanomaterial, Angew. Chem. Int. Ed. 48 (42) (2009) 7752–7777.
[31] M.S. Marshall, D.T. Newell, D.J. Payne, R.G. Egdell, M.R. Castell, Atomic and electronic surface structures of dopants in oxides: STM and XPS of Nb-and La-doped SrTiO 3 (001), Phys. Rev. B 83 (3) (2011), 035410.
[32] B. Bharti, S. Kumar, H.N. Lee, R. Kumar, Formation of oxygen vacancies and Ti 3+ state in TiO 2 thin film and enhanced optical properties by air plasma treatment, Sci. Rep. 6 (1) (2016) 1–12.
[33] C.D. Wagner, NIST X-Ray Photoelectron Spectroscopy Database, NIST Standarad Reference Database, 2000.
[34] S. Bhaskar, D. Allgeyer, J.A. Smythe III, Depth profiling of dielectric Sr Ti O 3 thin films by angle-resolved x-ray photoelectron spectroscopy, Appl. Phys. Lett. 89 (25) (2006), 254103.
[35] C. Chu, J. Wu, S. Yung, T. Chin, T. Zhang, F. Wu, Optical and structural properties of Sr–Nb–phosphate glasses, J. Non-Cryst. Solids 357 (3) (2011) 939–945.
[36] Y. Ando, X. Zhao, H. Shimoyama, G. Sakai, K. Kaneto, Physical properties of multiwalled carbon nanotubes, Int. J. Inorg. Mater. 1 (1) (1999) 77–82.
[37] M.F. De Volder, S.H. Tawfick, R.H. Baughman, A.J. Hart, Carbon nanotubes: present and future commercial applications, Science 339 (6119) (2013) 535–539.

[38] S. Ohta, T. Nomura, H. Ohta, K. Koumoto, High-temperature carrier transport and thermoelectric properties of heavily La-or Nb-doped Sr Ti O 3 single crystals, J. Appl. Phys. 97 (3) (2005), 034106.
[39] S.D. Kang, G.J. Snyder, Transport Property Analysis Method for Thermoelectric Materials: Material Quality Factor and the Effective Mass Model, *arXiv preprint arXiv* (2017).
[40] S.D. Kang, G.J. Snyder, Charge-transport model for conducting polymers, Nat. Mater. 16 (2) (2017) 252–257.
[41] Y. Xiao, H. Wu, J. Cui, D. Wang, L. Fu, Y. Zhang, Y. Chen, J. He, S.J. Pennycook, L. D. Zhao, Realizing high performance n-type PbTe by synergistically optimizing effective mass and carrier mobility and suppressing bipolar thermal conductivity, Energy Environ. Sci. 11 (9) (2018) 2486–2495.
[42] G.J. Snyder, A.H. Snyder, M. Wood, R. Gurunathan, B.H. Snyder, C. Niu, Weighted mobility, Adv. Mater. 32 (25) (2020), 2001537.
[43] J.U. Rahman, N. Van Du, W.H. Nam, W.H. Shin, K.H. Lee, W.S. Seo, M.H. Kim, S. Lee, Grain boundary interfaces controlled by reduced graphene oxide in nonstoichiometric SrTiO3-δ Thermoelectrics, Sci. Rep. 9 (1) (2019) 1–12.
[44] Y. Lin, M.T. Dylla, J.J. Kuo, J.P. Male, I.A. Kinloch, R. Freer, G.J. Snyder, Graphene/strontium titanate: approaching single crystal–like charge transport in polycrystalline oxide perovskite nanocomposites through grain boundary engineering, Adv. Funct. Mater. 30 (12) (2020), 1910079.
[45] C. Wu, J. Li, Y. Fan, J. Xing, H. Gu, Z. Zhou, X. Lu, Q. Zhang, L. Wang, W. Jiang, The effect of reduced graphene oxide on microstructure and thermoelectric properties of Nb-doped A-site-deficient SrTiO3 ceramics, J. Alloys Compd. 786 (2019) 884–893.
[46] S. Ohta, T. Nomura, H. Ohta, K. Koumoto, High-temperature carrier transport and thermoelectric properties of heavily La-or Nb-doped Sr Ti O 3 single crystals, J. Appl. Phys. 97 (3) (2005), 034106.
[47] P. Roy, V. Waghmare, T. Maiti, Environmentally friendly Ba x Sr 2− x TiFeO 6 double perovskite with enhanced thermopower for high temperature thermoelectric power generation, RSC Adv. 6 (60) (2016) 54636–54643.
[48] M. Saxena, K. Balani, T. Maiti, Structure and thermoelectric properties of calcium doped Sr2TiCoO6 double perovskites, Mater. Sci. Eng., B 244 (2019) 65–71.
[49] M. Saxena, T. Maiti, Effect of Ba-doping on high temperature thermoelectric properties of Sr2TiMoO6 double perovskites, J. Alloys Compd. 710 (2017) 472–478.
[50] J.A. Bock, S. Trolier-McKinstry, G.D. Mahan, C.A. Randall, Polarization-based perturbations to thermopower and electronic conductivity in highly conductive tungsten bronze structured (Sr, Ba) Nb 2 O 6: relaxors vs normal ferroelectrics, Phys. Rev. B 90 (11) (2014), 115106.
[51] S. Lee, G. Yang, R.H. Wilke, S. Trolier-McKinstry, C.A. Randall, Thermopower in highly reduced n-type ferroelectric and related perovskite oxides and the role of heterogeneous nonstoichiometry, Phys. Rev. B 79 (13) (2009), 134110.
[52] Y. Lin, C. Norman, D. Srivastava, F. Azough, L. Wang, M. Robbins, K. Simpson, R. Freer, I.A. Kinloch, Thermoelectric power generation from lanthanum strontium titanium oxide at room temperature through the addition of graphene, ACS Appl. Mater. Interfaces 7 (29) (2015) 15898–15908.
[53] P.A. Cox, Transition Metal Oxides: an Introduction to Their Electronic Structure and Properties, Oxford university press, 2010.
[54] P.W. Anderson, Absence of diffusion in certain random lattices, Phys. Rev. 109 (5) (1958) 1492.
[55] P. Bernasconi, I. Biaggio, M. Zgonik, P. Günter, Anisotropy of the electron and hole drift mobility in KNbO 3 and BaTiO 3, Phys. Rev. Lett. 78 (1) (1997) 106.
[56] H. Ihrig, D. Hennings, Electrical transport properties of n-type BaTi O 3, Phys. Rev. B 17 (12) (1978) 4593.
[57] C.T. White, T.N. Todorov, Carbon nanotubes as long ballistic conductors, Nature 393 (6682) (1998) 240–242.
[58] T. Dürkop, S.A. Getty, E. Cobas, M. Fuhrer, Extraordinary mobility in semiconducting carbon nanotubes, Nano Lett. 4 (1) (2004) 35–39.
[59] A. Javey, H. Kim, M. Brink, Q. Wang, A. Ural, J. Guo, P. McIntyre, P. McEuen, M. Lundstrom, H. Dai, High-κ dielectrics for advanced carbon-nanotube transistors and logic gates, Nat. Mater. 1 (4) (2002) 241–246.
[60] A. Javey, R. Tu, D.B. Farmer, J. Guo, R.G. Gordon, H. Dai, High performance n-type carbon nanotube field-effect transistors with chemically doped contacts, Nano Lett. 5 (2) (2005) 345–348.
[61] C. Kittel, P. McEuen, P. McEuen, Introduction to Solid State Physics, Wiley New York1996.
[62] B. Wei, R. Vajtai, P. Ajayan, Reliability and current carrying capacity of carbon nanotubes, Appl. Phys. Lett. 79 (8) (2001) 1172–1174.
[63] H.S. Kim, Z.M. Gibbs, Y. Tang, H. Wang, G.J. Snyder, Characterization of Lorenz number with Seebeck coefficient measurement, Apl. Mater. 3 (4) (2015), 041506.
[64] O. Okhay, S. Zlotnik, W. Xie, K. Orlinski, M.J.H. Gallo, G. Otero-Irurueta, A. J. Fernandes, D.A. Pawlak, A. Weidenkaff, A. Tkach, Thermoelectric performance of Nb-doped SrTiO3 enhanced by reduced graphene oxide and Sr deficiency cooperation, Carbon 143 (2019) 215–222.
[65] W.H. Nam, Y.S. Lim, W. Kim, H.K. Seo, K.S. Dae, S. Lee, W.S. Seo, J.Y. Lee, A gigantically increased ratio of electrical to thermal conductivity and synergistically enhanced thermoelectric properties in interface-controlled TiO 2–RGO nanocomposites, Nanoscale 9 (23) (2017) 7830–7838.
[66] P. Dey, S.S. Jana, F. Anjum, T. Bhattacharya, T. Maiti, Effect of semiconductor to metal transition on thermoelectric performance in oxide nanocomposites of SrTi0. 85Nb0. 15O3 with graphene oxide, Appl. Mater. Today 21 (2020), 100869.
[67] A. Ioffe, Semiconductor Thermoelements, and Thermoelectric, Cool-ingInfosearch Ltd., London, UK, 1957.